HARMONIC UNPAIRED IMAGE-TO-IMAGE TRANSLATION

Anonymous authors
Paper under double-blind review

ABSTRACT

The recent direction of unpaired image-to-image translation is on one hand very exciting as it alleviates the big burden in obtaining label-intensive pixel-to-pixel supervision, but it is on the other hand not fully satisfactory due to the presence of artifacts and degenerated transformations. In this paper, we take a manifold view of the problem by introducing a smoothness constraint over the sample graph to attain harmonic functions to enforce consistent mappings during the translation. We develop HarmonicGAN to learn bi-directional translations between the source and the target domain. With the help of similarity-consistency, the inherent self-consistency property of samples can be maintained. Distance metrics defined on two types of features including histogram and CNN are exploited. Under an identical problem setting as CycleGAN without additional manual inputs, HarmonicGAN demonstrates a significant qualitative and quantitative improvement over the state of the art, as well as improved interpretability. We show experimental results in a number of applications including medical imaging, object transfiguration, and semantic labeling. We outperform the competing methods in all tasks, and for a medical imaging task in particular our method turns CycleGAN from a failure to a success, halving the mean-squared error, and generating images that radiologists prefer over competing methods in 95% of cases.

1 INTRODUCTION

Image-to-image translation (Isola et al., 2017) aims to learn a mapping from a source domain to a target domain. As a significant and challenging task in computer vision, image-to-image translation benefits many vision and graphics tasks, such as realistic image synthesis (Isola et al., 2017; Zhu et al., 2017a), medical image generation (Zhang et al., 2018; Dar et al., 2018), and domain adaptation (Hoffman et al., 2018). Given a pair of training images with detailed pixel-to-pixel correspondences between the source and the target, image-to-image translation can be cast as a regression problem using e.g. Fully Convolutional Neural Networks (FCNs) (Long et al., 2015) by minimizing e.g. the per-pixel prediction loss. Recently, approaches using rich generative models based on Generative Adaptive Networks (GANs) (Goodfellow et al., 2014; Radford et al., 2016; Arjovsky et al., 2017) have achieved astonishing success. The main benefit of introducing GANs (Goodfellow et al., 2014) to image-to-image translation (Isola et al., 2017) is to attain additional image-level (often through patches) feedback about the overall quality of the translation, information which is not directly accessible through training the per-pixel regression objective.

The method by Isola et al. (2017) is able to generate high-quality images, but it requires paired training data which is difficult to collect and often does not exist. To perform translation without paired data, circularity-based approaches (Zhu et al., 2017a; Kim et al., 2017; Yi et al., 2017) have been proposed to learn translations of a set to another set, using a circularity constraint to establish relationships between the source and target domain and forcing the result generated from a sample in the source domain to map back to generate the original sample. The original image-to-image translation problem (Isola et al., 2017) is supervised at the pixel-level, whereas the unpaired image-to-image task (Zhu et al., 2017a) is considered unsupervised, with pixel-level supervision absent but with adversarial supervision at the image-level (in the target domain) present. By using a cycled regression for the pixel-level prediction (source→target→source) plus a term for the adversarial difference between the transferred images and the target images, CycleGAN is able to successfully, in many cases, train a translation model without paired source→target supervision. However, lacking

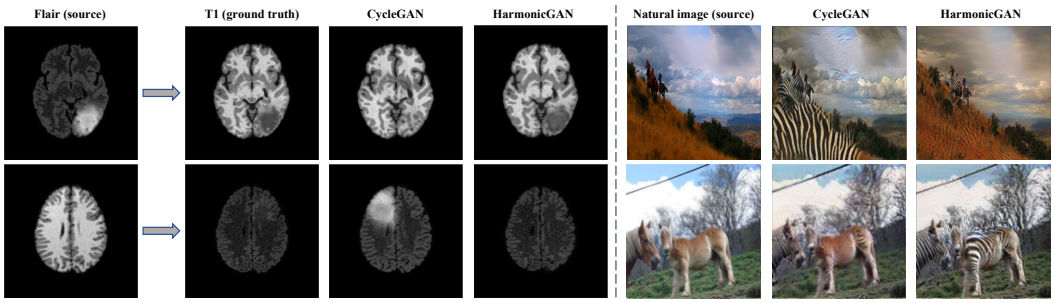

(a) (b)

Figure 1: HarmonicGAN corrects major failures in multiple domains: (a) for medical images it corrects incorrectly removed (top) and added (bottom) tumors; and (b) for horse $\rightarrow$ zebra transfiguration it does not incorrectly transform the background (top) and performs a complete translation (bottom).

a mechanism to enforce regularity in the translation creates problems like in Fig (1.a) and Fig 2, making undesirable changes to the image contents, superficially removing tumors (the first row) or creating tumors (the second row) at the wrong positions in the target domain. Fig (1.b) also shows some artifacts of CycleGAN on natural images when translating horses into zebras.

To combat the above issue, in this paper we look at the problem of unpaired image-to-image translation from a manifold learning perspective (Tenenbaum et al., 2000; Roweis & Saul, 2000). Intuitively, the problem can be alleviated by introducing a regularization term in the translation, encouraging similar contents (based on textures or semantics) in the same image to undergo similar translations/transformations. A common principle in manifold learning is to preserve local distances after the unfolding: forcing neighboring (similar) samples in the original space to be neighbors in the new space. The same principle has been applied to graph-based semi-supervised learning (Zhu, 2006) where harmonic functions with graph Laplacians (Zhu et al., 2003; Belkin et al., 2006) are used to obtain regularized labels of unlabeled data points.

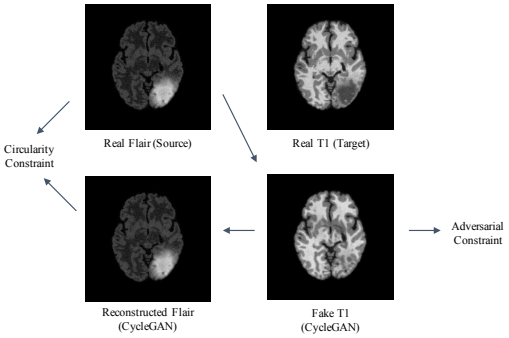

Figure 2: For CycleGAN, the translated image may perfectly match the input under the circularity constraint while not maintaining the inherent property of the source image (e.g. a tumor), thus generating unexpected results (e.g. incorrectly removing a tumor).

During the translation/transformation, some domain-specific attributes are changed, such as the colors, texture, and semantics of certain image regions (see e.g. the examples in Fig 1). Although there is no supervised information for these changes, certain consistency during the transformation is desirable. Inspired by graph-based semi-supervised learning (Zhu et al., 2003; Zhu, 2006), we introduce smoothness constraints to unpaired image-to-image translation (Zhu et al., 2017a) by providing a stronger regularization for the translation/transformation between the source and target domains, aiming to exploit the "manifold structure" of the source and target domains. For a pair of similar samples (two different locations in an image; one can think of them as two patches although the receptive fields of CNN are quite large), we add a smoothness constraint to minimize a weighted distance of the corresponding locations in the target image. Note that two spatially distant samples might be neighbors in the feature space. We name our algorithm **HarmonicGAN** as it behaves harmonically along with the circularity and adversarial constraints to learn a pair of dual translations between the source and the target domains. Metrics defined on two alternative features are adopted: (1) a low-level soft RGB histograms; and (2) CNN (VGG) features with pre-trained semantics.

We conduct experiments in a number of applications, showing that in each of them our method outperforms existing methods quantitatively, qualitatively, and with user studies. For a medical imaging task (Cohen et al., 2018) that was recently calling attention to a major CycleGAN failure case (learning to accidentally add/remove tumors in an MRI image translation task), our proposed method provides a large improvement over CycleGAN, halving the mean-squared error, and generating images that radiologists prefer over competing methods in 95% of cases.

CONTRIBUTIONS

1. We introduce smooth regularization over the graph for unpaired image-to-image translation to attain harmonic translations.
2. When building an end-to-end learning pipeline, we adopt two alternative types of feature measures to compute the weight matrix for the graph Laplacian, one based on a soft histogram (Wang et al., 2016) and another based on semantic CNN (VGG) features (Simonyan & Zisserman, 2015).
3. We show that this results in significantly improved consistency for transformations. With experiments on multiple translation tasks, we demonstrate that HarmonicGAN outperforms the state of the art.

2 RELATED WORK

As discussed in the introduction, the general image-to-image translation task in the deep learning era was pioneered by Isola et al. (2017), but there are prior works such as image analogies (Hertzmann et al., 2001) that aim at a similar goal, along with other exemplar-based methods (Efros & Freeman, 2001; Criminisi et al., 2004; Barnes et al., 2009). After (Isola et al., 2017), a series of other works have also exploited pixel-level reconstruction constraints to build connections between the source and target domain (Zhang et al., 2017; Wang et al., 2018). The image-to-image translation framework (Isola et al., 2017) is very powerful but it requires a sufficient amount of training data with paired source to target images, which are often laborious to obtain in the general tasks such as labeling, synthesis (Chen & Koltun, 2017), and style transfer (Huang & Belongie, 2017).

Unpaired image-to-image translation frameworks (Zhu et al., 2017a;b; Liu et al., 2017; Shrivastava et al., 2017; Kim et al., 2017) such as CycleGAN remove the requirement of having detailed pixel-level supervision. In CycleGAN this is achieved by enforcing a bi-directional prediction from source to target and target back to source, with an adversarial penalty in the translated images in the target domain. Similar unsupervised circularity-based approaches (Kim et al., 2017; Yi et al., 2017) have also been developed. The CycleGAN family models (Zhu et al., 2017a;b) point to an exciting direction of unsupervised approaches but they also create artifacts in many applications. As shown in Fig 2, one reason for this is that the circularity constraint in CycleGAN lacks the straightforward description of the target domain, so it may change the inherent properties of the original samples and generate unexpected results which are inconsistent at different image locations. These failures have been prominently explored in recent works, showing that CycleGAN (Zhu et al., 2017a) may add or remove tumors accidentally in cross-modal medical image synthesis (Cohen et al., 2018), and that in the task of natural image transfiguration, e.g. from a horse to zebra, regions in the background may also be translated into a zebra-like texture (Zhu et al., 2018) (see Fig 1).

Here we propose HarmonicGAN that introduces a smoothness term into the CycleGAN framework to enforce a regularized translation, enforcing similar image content in the source space to also be similar in the target space. We follow the general design principle in manifold learning (Tenenbaum et al., 2000; Roweis & Saul, 2000) and the development of harmonic functions in the graph-based semi-supervised learning literature (Zhu et al., 2003; Belkin et al., 2006; Zhu, 2006). There has been previous work, DistanceGAN (Benaim & Wolf, 2017), in which distance preservation was also implemented. However, DistanceGAN differs from HarmonicGAN in (1) motivation, (2) formulation, (3) implementation, and (4) performance. The primary motivation of DistanceGAN was to demonstrate an alternative loss term for the per-pixel difference in CycleGAN. The practical gain of DistanceGAN over CycleGAN is however not clear. We observe that the cycled per-pixel loss in CycleGAN is effective and we aim to make the translation harmonic by introducing additional regularization. The smoothness term acts as a graph Laplacian imposed on all pairs of samples (using random samples in the implementation). In the experimental results, we show that the artifacts in CycleGAN are still present in DistanceGAN, whereas HarmonicGAN provides a significant boost to the performance of CycleGAN.

3 HARMONICGAN FOR UNPAIRED IMAGE-TO-IMAGE TRANSLATION

Following the basic formulation in CycleGAN (Zhu et al., 2017a), for the source domain X and target domain Y, we consider unpaired training samples $\{x_k\}_{k=1}^N$ where $x_k \in X$, and $\{y_k\}_{k=1}^N$ where $y_k \in Y$. The goal of image-to-image translation is to learn a pair of dual mappings, including forward mapping $G : X \to Y$ and backward mapping $F : Y \to X$. Two discriminators D_X and

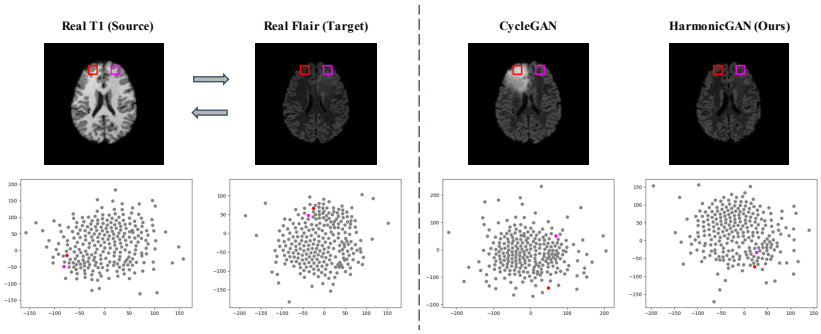

Figure 3: Visualization using t-SNE (Maaten & Hinton, 2008) to illustrate the effectiveness of the smoothness constraint in HarmonicGAN (best viewed in color). Left: For two similar patches in the original sample, if the translation maintains the non-tumor property of these two patches in the translated sample then the two patches will also be similar in the source space. Right: For two similar patches in the original sample, if one patch is translated to a tumor region while the other is not, the two patches will have a large distance in the target space, resulting in a translation that incorrectly adds a tumor into the original sample.

D_Y are adopted in Zhu et al. (2017a) to distinguish between real images and generated images. In particular, the discriminator D_X aims to distinguish real image $\{x\}$ from the generated image $\{F(y)\}$, while the discriminator D_Y aims to distinguish real image $\{y\}$ from the generated image $\{G(x)\}$.

Therefore, the objective of adversarial constraints are applied in both source and target domains, expressed in Zhu et al. (2017a) as:

$$\mathcal{L}_{\text{GAN}}(G, D_Y, X, Y) = \mathbb{E}_{y \in Y}[\log D_Y(y)] + \mathbb{E}_{x \in X}[\log(1 - D_Y(G(x)))], \tag{1}$$

and

$$\mathcal{L}_{\text{GAN}}(F, D_X, X, Y) = \mathbb{E}_{x \in X}[\log D_X(x)] + \mathbb{E}_{y \in Y}[\log(1 - D_x(F(y)))]. \tag{2}$$

For notational simplicity, we denote the GAN loss as

$$\mathcal{L}_{\text{GAN}}(G, F) = \arg \max_{D_Y, D_X} [\mathcal{L}_{\text{GAN}}(G, D_Y, X, Y) + \mathcal{L}_{\text{GAN}}(F, D_X, X, Y)]. \tag{3}$$

Since the data in the two domains are unpaired, a circularity constraint is introduced in Zhu et al. (2017a) to establish a relationships between X and Y. The circularity constraint enforces that the mappings G and F are a pair of inverse mappings, and that the translated sample can be mapped back to the original sample. The circularity constraint contains consistencies in two aspects: the forward cycle $x \to G(X) \to F(G(x)) \sim x$ and the backward cycle $y \to F(y) \to G(F(y)) \sim y$. Thus, the circularity constraint is formulated as (Zhu et al., 2017a):

$$\mathcal{L}_{\text{cyc}}(G, F) = \mathbb{E}_{x \in X}||F(G(x)) - x||_1 + \mathbb{E}_{y \in Y}||G(F(y)) - y||_1. \tag{4}$$

Here we rewrite the overall objective in Zhu et al. (2017a) to minimize as:

$$\mathcal{L}_{\text{CycleGAN}}(G, F) = \lambda_{\text{GAN}} \times \mathcal{L}_{\text{GAN}}(G, F) + \lambda_{\text{cyc}} \times \mathcal{L}_{\text{cyc}}(G, F), \tag{5}$$

where the weights λ_{GAN} and λ_{cyc} control the importance of the corresponding objectives.

3.1 Smoothness constraint over the graph

The full objective of circularity-based approach contains adversarial constraints and a circularity constraint. The adversarial constraints ensure the generated samples are in the distribution of the source or target domain, but ignore the relationship between the input and output of the forward or backward translations. The circularity constraint establishes connections between the source and target domain by forcing the forward and backward translations to be the inverse of each other. However, CycleGAN has limitations: as shown in Fig 2, the circular projection might perfectly match the input, and the translated image might look very well like a real one, but the translated image may contain a large artifact that is not connected to the source image.

Here we propose a smoothness constraint to enforce a stronger correlation between the source and target domains that focuses on providing similarity-consistency between image patches during the translation. For any image $x \in X$, we define the set that consists of individual samples (can be

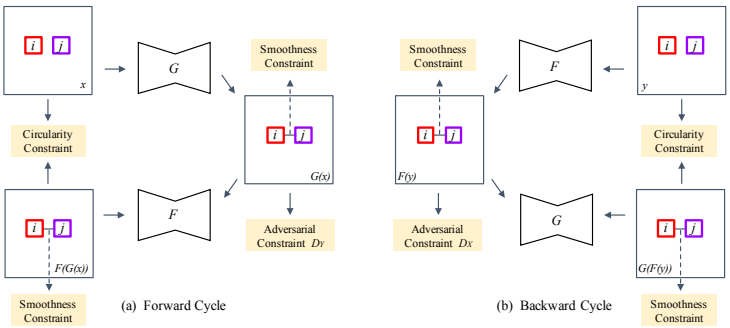

Figure 4: Architecture of HarmonicGAN, consisting of a pair of inverse generators G, F and two discriminators D_X, D_Y. The objective combines an adversarial constraint, circularity constraint and smoothness constraint.

viewed as image patches) of image x as $S = \{x(i), i = 1..M\}$ where M is the total number of the samples/patches. An affinity measure (similarity) computed on image patch $x(i)$ and image patch $x(j)$, w_{ij}, defines the edge on the graph of $\mathcal{G}$ of S. Therefore, we define a smoothness constraint over the graph as

$$\mathcal{L}_{\text{Smooth}}(G,X,Y)=\mathbb{E}_{x\in X}\left[\sum_{i,j} w_{ij}(x)\times Dist[G(x)(i),G(x)(j)]+\sum_{i,j} w_{ij}(G(x))\times Dist[F(G(x))(i),F(G(x))(j)]\right], \tag{6}$$

where $w_{ij}(x) = \exp\{-Dist[x(i), x(j)]/\sigma^2\}$ (Zhu et al., 2003) defines the affinity between two patches $x(i)$ and $x(j)$ based on their distances (e.g. Histogram or CNN features). $Dist[G(Y)(i), G(Y)(i)]$ defines the distance between two image patches after translation at the same locations. Similarly, we define a smoothness constraint for the backward part as

$$\mathcal{L}_{\text{Smooth}}(F,Y,X)=\mathbb{E}_{y\in Y}\left[\sum_{i,j} w_{ij}(y)\times Dist[F(y)(i),F(y)(j)]+\sum_{i,j} w_{ij}(F(y))\times Dist[G(F(y))(i),G(F(y))(j)]\right], \tag{7}$$

The combined loss for the smoothness thus becomes

$$\mathcal{L}_{\text{Smooth}}(G, F) = \mathcal{L}_{\text{Smooth}}(G, X, Y) + \mathcal{L}_{\text{Smooth}}(F, Y, X). \tag{8}$$

3.2 Overall objective function

As shown in Figure 4, HarmonicGAN consists of a pair of inverse generators G, F and two discriminators D_X, D_Y, defined in Eqn. (1) and Eqn. (2). The full objective combines an adversarial constraint (see Eqn. (3)), circularity constraint (see Eqn. (4)), and smoothness constraint (see Eqn. (8)). The adversarial constraint forces the translated images to be plausible and indistinguishable from the real images; the circularity constraint ensures the cycle-consistency of translated images; and the smoothness constraint provides a stronger similarity-consistency between patches to maintain inherent properties of the images.

Combining Eqn. (5) and Eqn. (8), the **overall objective** for our proposed HarmonicGAN under the smoothness constraint becomes

$$\mathcal{L}_{\text{HarmonicGAN}}(G, F) = \mathcal{L}_{\text{CycleGAN}}(G, F) + \lambda_{smooth} \times \mathcal{L}_{\text{Smooth}}(G, F). \tag{9}$$

Similar to the graph-based semi-supervised learning definition (Zhu et al., 2003; Zhu, 2006), the solution to Eqn. (9) leads to a harmonic function. The optimization process during training obtains:

$$G^*, F^* = \arg\min_{G,F} \mathcal{L}_{\text{HarmonicGAN}}(G, F). \tag{10}$$

The effectiveness of the smoothness term of Eqn. (8) is evident. In Fig 7, we show (using t-SNE (Maaten & Hinton, 2008)) that the local neighborhood structure is being preserved by HarmonicGAN, whereas CycleGAN results in two similar patches being far apart after translation.

3.3 Feature design

In the smoothness constraint, the similarity of a pair of patches is measured on the features for each patch (sample point). All the patches in an image form a graph. Here we adopt two types of features: (1) a low-level soft histogram, and (2) pre-trained CNN (VGG) features that carry semantic information. Soft histogram features are lightweight and easy to implement but without much semantic information; VGG requires an additional CNN network but carries more semantics.

3.3.1 SOFT RGB HISTOGRAM FEATURES

We first design a weight matrix based on simple low-level RGB histograms. To make the end-to-end learning system work, it is crucial to make the computation of gradient in the histograms derivable. We adopt a soft histogram representation proposed in Wang et al. (2016) but fix the means and the bin size. This soft histogram function contains a family of linear basis functions $\psi_b, b = 1, \ldots, B$, where B is the number of bins in the histogram. Suppose P_x^i represents the patch i in image x. For each pixel j in P_x^i, $\psi_b(P_x^i(j)$ represents the pixel j voting for the b-th bin, expressed as:

$$\psi_b(P_x^i(j)) = \max\{0, 1 - |P_x^i(j) - \mu_b| \times w_b\}, \tag{11}$$

where μ_b and w_b are the center and width of the b-th bin. The representation of P_x^i in the RGB space is the linear combination of linear basis functions on all the pixels in P_x^i, expressed as:

$$\phi_h(x, i, b) = \phi_h(P_x^i, b) = \sum_j \psi_b(P_x^i(j)), \tag{12}$$

where ϕ_h is the RGB histogram feature, b is the index of dimension of the RGB histogram representation, and j represents any pixel in the patch P_x^i. The RGB histogram representation $\phi_h(x, i)$ of P_x^i is a B-dimensional vector.

3.3.2 SEMANTIC CNN FEATURES

For some domains we instead use semantic features to acquire higher-level representations of patches. The semantic representations are extracted from a pre-trained Convolutional Neural Network (CNN). The CNN encodes semantically relevant features from training on a large-scale dataset. It extracts semantic information of local patches in the image through multiple pooling or stride operators. Each point in the feature maps of the CNN is a semantic descriptor of the corresponding image patch. Additionally, the semantic features learned from the CNN are differentiable and the CNN can be integrated into the GAN and be trained end-to-end. In practice we instantiate the semantic feature ϕ_s as as a pre-trained CNN model e.g. VGGNet (Simonyan & Zisserman, 2014).

4 EXPERIMENTS

We evaluate the proposed method on three different applications: medical imaging, semantic labeling, and object transfiguration. We compare against several unpaired image-to-image translation methods: CycleGAN (Zhu et al., 2017a), DiscoGAN (Kim et al., 2017), DistanceGAN (Benaim & Wolf, 2017), and UNIT (Liu et al., 2017). We also provide two user studies as well as qualitative results. The appendix provides implementation details and additional results.

4.1 DATASETS AND EVALUATION METRICS

Medical imaging. This task evaluates cross-modal medical image synthesis, Flair $\leftrightarrow$ T1. The models are trained on the BRATS dataset (Menze et al., 2015) which contains paired MRI data to allow quantitative evaluation. Similar to previous work (Cohen et al., 2018), we use a training set of 1700 image slices (50% healthy and 50% tumors) and a test set of 300, and use their unpaired training scenario. We adopt the Mean Absolute Error (MAE) and the Mean Squared Error (MSE) between the generated images and the real images to evaluate the reconstruction errors, and further use the Peak Signal-to-Noise Ratio (PSNR) and Structural Similarity Index Measure (SSIM) to evaluate the reconstruction quality of generated images.

Semantic labeling. We also test our method on the labels $\leftrightarrow$ photos task using the Cityscapes dataset (Cordts et al., 2016) under the unpaired setting as in the original CycleGAN paper. For quantitative evaluation, in line with previous work, for labels $\rightarrow$ photos we adopt the "FCN score" (Isola et al., 2017), which evaluates how interpretable the generated photos are according to a semantic segmentation algorithm. For photos $\rightarrow$ labels, we use the standard segmentation metrics, including per-pixel accuracy, per-class accuracy, and mean class Intersection-Over-Union (Class IOU).

Object transfiguration. Finally, we test our method on the horse $\leftrightarrow$ zebra task using the standard CycleGAN dataset (2401 training images, 260 test images). This task does not have a quantitative evaluation measure, so we instead provide a user study together with qualitative results.

4.2 QUANTITATIVE COMPARISON

Medical imaging. Table 1 shows the reconstruction performance on medical image synthesis, Flair ↔ T1. The proposed method yields a large improvement over CycleGAN, showing lower MAE and MSE reconstruction losses, and higher PSNR and SSIM reconstruction scores, highlighting the significance of the proposed smoothness regularization. HarmonicGAN based on histogram and VGG features shows similar performance; the reconstruction losses of histogram-based HarmonicGAN are slightly lower than the VGG-based one in Flair → T1, while they are slightly higher in T1 → Flair, indicating that both low-level RGB values and high-level CNN features can represent the inherent property of medical images well and help to maintain the self-consistency of samples.

Table 1: Reconstruction evaluation of cross-modal medical image synthesis on the BRATS dataset.

Method	Flair → T1				T1 → Flair			
	MAE ↓	MSE ↓	PSNR ↑	SSIM ↑	MAE ↓	MSE ↓	PSNR ↑	SSIM ↑
CycleGAN	10.47	674.40	22.35	0.80	11.81	1026.19	18.73	0.74
DiscoGAN	10.63	641.35	20.06	0.79	10.66	839.15	19.14	0.69
DistanceGAN	14.93	1197.64	17.92	0.67	10.57	716.75	19.95	0.64
UNIT	9.48	439.33	22.24	0.76	6.69	261.26	25.11	**0.76**
HarmonicGAN (ours)								
Histogram	**6.38**	**216.83**	**24.34**	**0.83**	5.04	163.29	26.72	0.75
VGG	6.86	237.94	24.14	0.81	**4.69**	**127.84**	**27.22**	**0.76**

Semantic labeling. We report both semantic labeling results in Table 2. The proposed method using VGG features yields a 3% improvement in Pixel Accuracy in translation scores for photo ↔ label and also shows stable improvements in other metrics, clearly outperforming all competing methods. The performance using a histogram is slight lower than CycleGAN; we hypothesize that the reason is that the objects in photos have a large intra-class variance and inter-class similarity in appearance, e.g. cars have different colors, while vegetation and terrain have similar colors, thus the regularization of the RGB histogram is not appropriate to extract the inherent property of photos.

Table 2: FCN scores of Photo ↔ Label translation on the Cityscapes dataset.

Method	Label → Photo			Photo → Label		
	Pixel Acc. ↑	Class Acc. ↑	Class IoU ↑	Pixel Acc. ↑	Class Acc. ↑	Class IoU ↑
CycleGAN	52.7	15.2	11.0	57.2	21.0	15.7
DiscoGAN	45.0	11.1	7.0	45.2	10.9	6.3
DistanceGAN	48.5	10.9	7.3	20.5	8.2	3.4
UNIT	48.5	12.9	7.9	56.0	20.5	14.3
HarmonicGAN (ours)						
Histogram	52.2	14.8	10.9	56.6	20.9	15.7
VGG	**55.9**	**17.6**	**13.3**	**59.8**	**22.1**	**17.2**

4.3 USER STUDIES

Medical imaging. We randomly selected 100 images from BRATS test set. For each image, we showed one radiologist the real ground truth image, followed by images generated by CycleGAN, DistanceGAN and HarmonicGAN (different order for each image set to avoid bias). The radiologist was told to evaluate similarity by how likely they would lead to the same clinical diagnosis, and was asked to rate similarity of the generation methods on a Likert scale from 1 to 5 (1 is not similar at all, 5 is exactly same). Results are in shown in Table 3. In 95% of cases, the radiologist preferred images generated by our method over the competing methods, and the average Likert score was 4.00 compared to 1.68 for CycleGAN, confirming that our generated images are significantly better. This is significant as it confirms that we solve the issue presented in a recent paper (Cohen et al., 2018) showing that CycleGAN can learn to accidentally add/remove tumors in images.

Table 3: User study on the BRATS dataset.

Metric	CycleGAN	DistanceGAN	HarmonicGAN
Prefer [%] ↑	5	0	**95**
Mean Likert ↑	1.68	1.62	**4.00**
Std Likert	0.99	0.95	0.88

Table 4: User study on the horse to zebra dataset.

Metric	CycleGAN	DistanceGAN	HarmonicGAN
Prefer[%]↑	28	0	**72**
Mean Likert ↑	3.16	1.08	**3.60**
Std Likert	0.81	0.23	0.78

Object transfiguration. We evaluate our algorithm on horse ↔ zebra with a human perceptual study. We randomly selected 50 images from the horse2zebra test set and showed the input images and three generated images from CycleGAN, DistanceGAN and HarmonicGAN (with generated images in a random order). 10 participants were asked to score the generated images on a Likert scale from 1 to 5 (as above). As shown in Table 4, the participants give the highest score to the proposed method (in 72% of cases), significantly more often than CycleGAN (in 28% of cases). Additionally, the average Likert score of our method was 3.60, outperforming 3.16 of CycleGAN and 1.08 of DistanceGAN, indicating that our method generates better results.

4.4 Qualitative Comparison

Medical imaging. Fig 5 shows the qualitative comparison of the proposed method (HarmonicGAN) and two baseline methods, CycleGAN and DistanceGAN, on Flair ↔ T1. It shows that both CycleGAN and DistanceGAN may remove tumors in the original images and add tumors to other locations in the brain. In contrast, our method preserves the location of tumors, confirming that the harmonic regularization can maintain the inherent property of tumor/non-tumor regions and solves the tumor add/remove problem introduced in Cohen et al. (2018).

Object transfiguration. Fig 5 shows a qualitative comparison of our method on the horse ↔ zebra task. We observe that we correct several problems in CycleGAN, including not changing the background and performing more complete transformations.

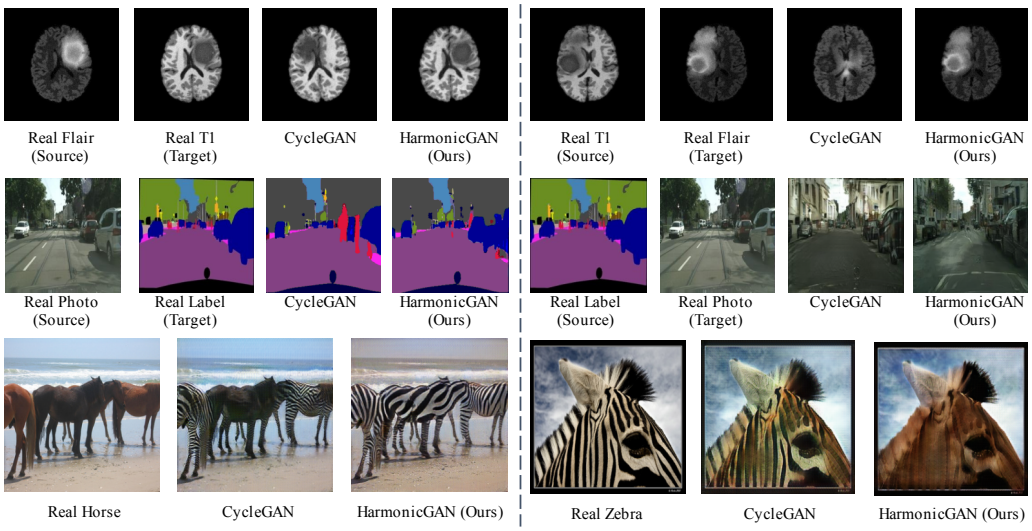

Figure 5: Qualitative comparison for BRATS, Cityscapes and horse ↔ zebra **(see appendix for more images)**.

5 Conclusion

We have shown that by introducing additional regularization to enforce consistent mappings during the image-to-image translation, the inherent self-consistency property of samples can be maintained. Through a set of quantitative, qualitative and user studies, we have demonstrated that this results in a significant improvement over the current state-of-the-art methods in a number of applications including medical imaging, object transfiguration, and semantic labeling. In a medical imaging task in particular our method provides a very significant improvement over CycleGAN.

REFERENCES

Martin Arjovsky, Soumith Chintala, and Léon Bottou. Wasserstein generative adversarial networks. In *ICML*, 2017.

Connelly Barnes, Eli Shechtman, Adam Finkelstein, and Dan B Goldman. Patchmatch: A randomized correspondence algorithm for structural image editing. *ACM Trans. Graphics (ToG)*, 2009.

Mikhail Belkin, Partha Niyogi, and Vikas Sindhwani. Manifold regularization: A geometric framework for learning from labeled and unlabeled examples. *JMLR*, 2006.

Sagie Benaim and Lior Wolf. One-sided unsupervised domain mapping. In *NIPS*, 2017.

Qifeng Chen and Vladlen Koltun. Photographic image synthesis with cascaded refinement networks. In *ICCV*, 2017.

Joseph Paul Cohen, Margaux Luck, and Sina Honari. Distribution matching losses can hallucinate features in medical image translation. In *MICCAI*, 2018.

Marius Cordts, Mohamed Omran, Sebastian Ramos, Timo Rehfeld, Markus Enzweiler, Rodrigo Benenson, Uwe Franke, Stefan Roth, and Bernt Schiele. The cityscapes dataset for semantic urban scene understanding. In *CVPR*, 2016.

Antonio Criminisi, Patrick Pérez, and Kentaro Toyama. Region filling and object removal by exemplar-based image inpainting. *IEEE Trans. image processing*, 2004.

Salman Ul Hassan Dar, Mahmut Yurt, Levent Karacan, Aykut Erdem, Erkut Erdem, and Tolga Çukur. Image synthesis in multi-contrast MRI with conditional generative adversarial networks. *arXiv preprint*, 2018.

Alexei A Efros and William T Freeman. Image quilting for texture synthesis and transfer. In *Proc. Computer graphics and interactive techniques*, 2001.

Ian J. Goodfellow, Jean Pouget-Abadie, Mehdi Mirza, Bing Xu, David Warde-Farley, Sherjil Ozair, Aaron C. Courville, and Yoshua Bengio. Generative adversarial nets. In *NIPS*, 2014.

Aaron Hertzmann, Charles E Jacobs, Nuria Oliver, Brian Curless, and David H Salesin. Image analogies. In *Proc. Computer graphics and interactive techniques*, 2001.

Judy Hoffman, Eric Tzeng, Taesung Park, Jun-Yan Zhu, Phillip Isola, Kate Saenko, Alexei A Efros, and Trevor Darrell. Cycada: Cycle-consistent adversarial domain adaptation. In *ICML*, 2018.

Xun Huang and Serge J Belongie. Arbitrary style transfer in real-time with adaptive instance normalization. In *ICCV*, 2017.

Phillip Isola, Jun-Yan Zhu, Tinghui Zhou, and Alexei A. Efros. Image-to-image translation with conditional adversarial networks. In *CVPR*, 2017.

Justin Johnson, Alexandre Alahi, and Li Fei-Fei. Perceptual losses for real-time style transfer and super-resolution. In *ECCV*, 2016.

Taeksoo Kim, Moonsu Cha, Hyunsoo Kim, Jung Kwon Lee, and Jiwon Kim. Learning to discover cross-domain relations with generative adversarial networks. In *ICML*, 2017.

Diederik P Kingma and Jimmy Ba. Adam: A method for stochastic optimization. In *ICLR*, 2015.

Ming-Yu Liu, Thomas Breuel, and Jan Kautz. Unsupervised image-to-image translation networks. In *NIPS*, 2017.

Jonathan Long, Evan Shelhamer, and Trevor Darrell. Fully convolutional networks for semantic segmentation. In *CVPR*, 2015.

Laurens van der Maaten and Geoffrey Hinton. Visualizing data using t-sne. *JMLR*, 2008.

Xudong Mao, Qing Li, Haoran Xie, Raymond YK Lau, Zhen Wang, and Stephen Paul Smolley. Least squares generative adversarial networks. In *ICCV*, 2017.

Bjoern H Menze, Andras Jakab, Stefan Bauer, Jayashree Kalpathy-Cramer, Keyvan Farahani, Justin Kirby, Yuliya Burren, Nicole Porz, Johannes Slotboom, Roland Wiest, et al. The multimodal brain tumor image segmentation benchmark (brats). *IEEE trans. medical imaging*, 2015.

Alec Radford, Luke Metz, and Soumith Chintala. Unsupervised representation learning with deep convolutional generative adversarial networks. In *ICLR*, 2016.

Sam T Roweis and Lawrence K Saul. Nonlinear dimensionality reduction by locally linear embedding. *Science*, 2000.

Ashish Shrivastava, Tomas Pfister, Oncel Tuzel, Joshua Susskind, Wenda Wang, and Russell Webb. Learning from simulated and unsupervised images through adversarial training. In *CVPR*, 2017.

Karen Simonyan and Andrew Zisserman. Very deep convolutional networks for large-scale image recognition. *arXiv preprint arXiv:1409.1556*, 2014.

Karen Simonyan and Andrew Zisserman. Very deep convolutional networks for large-scale image recognition. In *ICLR*, 2015.

Joshua B Tenenbaum, Vin De Silva, and John C Langford. A global geometric framework for nonlinear dimensionality reduction. *Science*, 2000.

Ting-Chun Wang, Ming-Yu Liu, Jun-Yan Zhu, Andrew Tao, Jan Kautz, and Bryan Catanzaro. High-resolution image synthesis and semantic manipulation with conditional gans. In *CVPR*, 2018.

Zhe Wang, Hongsheng Li, Wanli Ouyang, and Xiaogang Wang. Learnable histogram: Statistical context features for deep neural networks. In *ECCV*, 2016.

Zili Yi, Hao (Richard) Zhang, Ping Tan, and Minglun Gong. Dualgan: Unsupervised dual learning for image-to-image translation. In *ICCV*, 2017.

Han Zhang, Tao Xu, Hongsheng Li, Shaoting Zhang, Xiaolei Huang, Xiaogang Wang, and Dimitris Metaxas. StackGAN: Text to photo-realistic image synthesis with stacked generative adversarial networks. *arXiv preprint*, 2017.

Zizhao Zhang, Lin Yang, and Yefeng Zheng. Translating and segmenting multimodal medical volumes with cycle-and shapeconsistency generative adversarial network. In *CVPR*, 2018.

Jun-Yan Zhu, Taesung Park, Phillip Isola, and Alexei A Efros. Unpaired image-to-image translation using cycle-consistent adversarial networks. In *ICCV*, 2017a.

Jun-Yan Zhu, Richard Zhang, Deepak Pathak, Trevor Darrell, Alexei A Efros, Oliver Wang, and Eli Shechtman. Toward multimodal image-to-image translation. In *NIPS*, 2017b.

Jun-Yan Zhu, Taesung Park, Phillip Isola, and Alexei A Efros. CycleGAN failure cases. `https://github.com/junyanz/CycleGAN#failure-cases`, 2018.

Xiaojin Zhu. Semi-supervised learning literature survey. *Computer Science, University of Wisconsin-Madison*, 2006.

Xiaojin Zhu, Zoubin Ghahramani, and John D Lafferty. Semi-supervised learning using gaussian fields and harmonic functions. In *ICML*, 2003.

6 APPENDIX

6.1 IMPLEMENTATION DETAILS

We apply the proposed smoothness constrains on the framework of CycleGAN (Zhu et al., 2017a). Similar with CycleGAN, we adopt the architecture of Johnson et al. (2016) as the generator and the PatchGAN (Isola et al., 2017) as the discriminator. The log likelihood objective in the original GAN is replaced with a least-squared loss (Mao et al., 2017) for more stable training. We resize the input images to the size of 256×256. For the histogram feature, we equally split the RGB range of [0, 255] to 16 bins, each with a range of 16. Images are divided into non-overlapping patches of 8×8 and the histogram feature is computed on each patch. For the semantic feature, we adopt a VGG network pre-trained on ImageNet to obtain semantic features. We select the feature map of layer relu4_3 in VGG. The loss weights are set as $\lambda_{\text{GAN}} = \lambda_{\text{Smooth}} = 1$, $\lambda_{\text{cyc}} = 10$. Following CycleGAN, we adopt the Adam optimizer (Kingma & Ba, 2015) with a learning rate of 0.0002. The learning rate is fixed for the first 100 epochs and linearly decayed to zero over the next 100 epochs.

6.2 ADDITIONAL EXPERIMENTS

Figure 6: Comparison on horse ↔ zebra for the Putin photo. CycleGAN translates both the background and human to a zebra-like texture. In contrast, HarmonicGAN does better in background region and achieves an improvement in some regions of of the human (Putin's face), but it still fails on the human body. We hypothesize this is because the semantic features used by HarmonicGAN have not been trained on humans without a shirt.

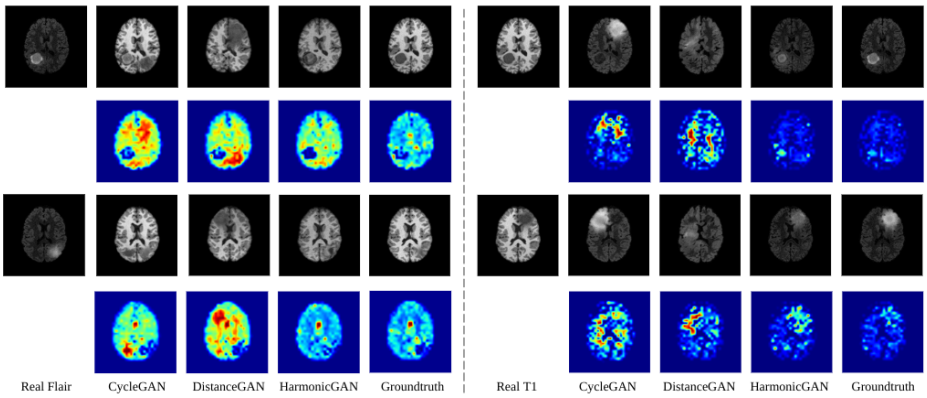

Figure 7: Visualizing results for cross-modal medical image synthesis on BRATS dataset. The distance of image patches in the target space shows the inconsistently translated patches.

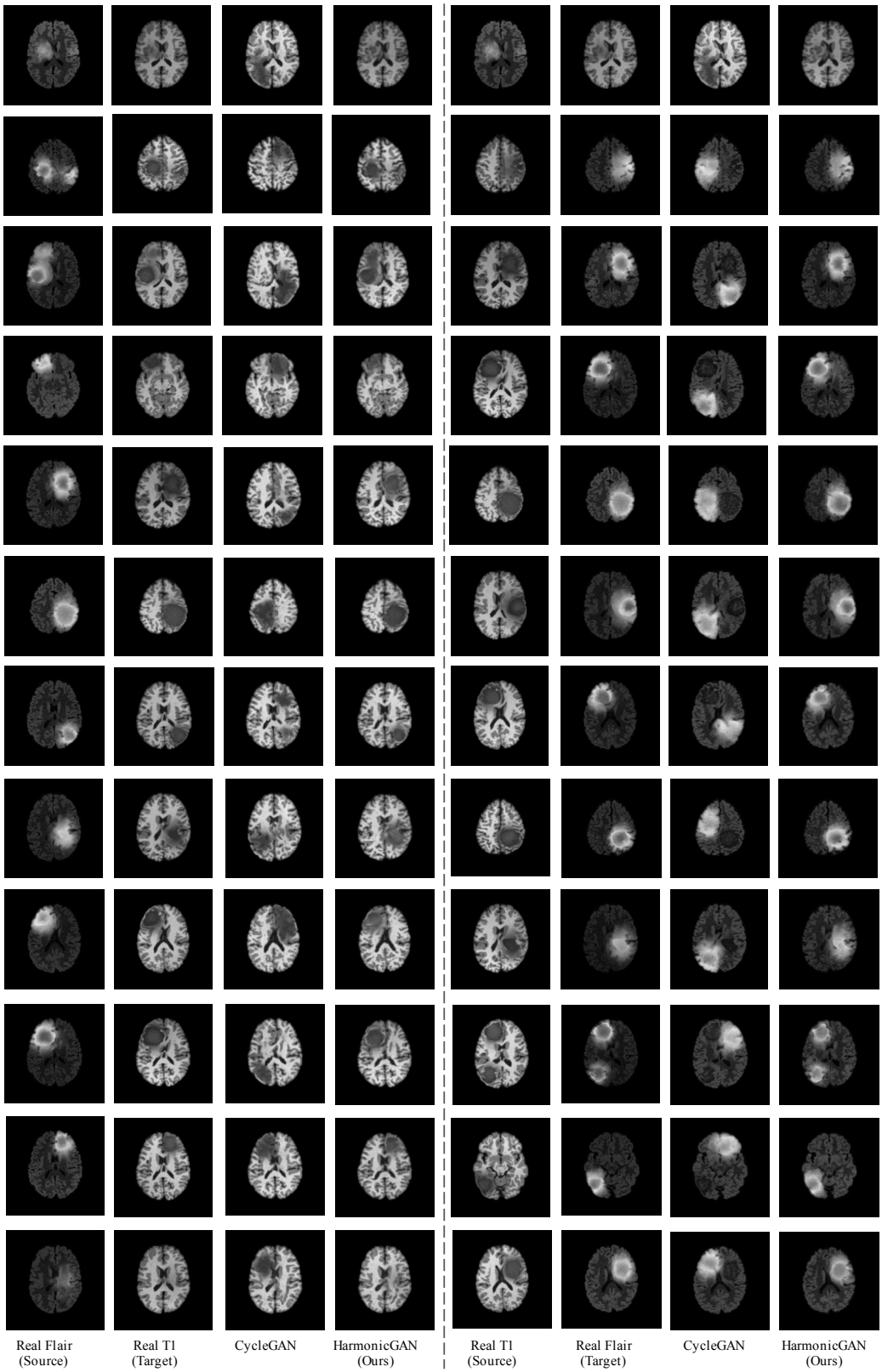

Figure 8: Comparison on BRATS dataset.

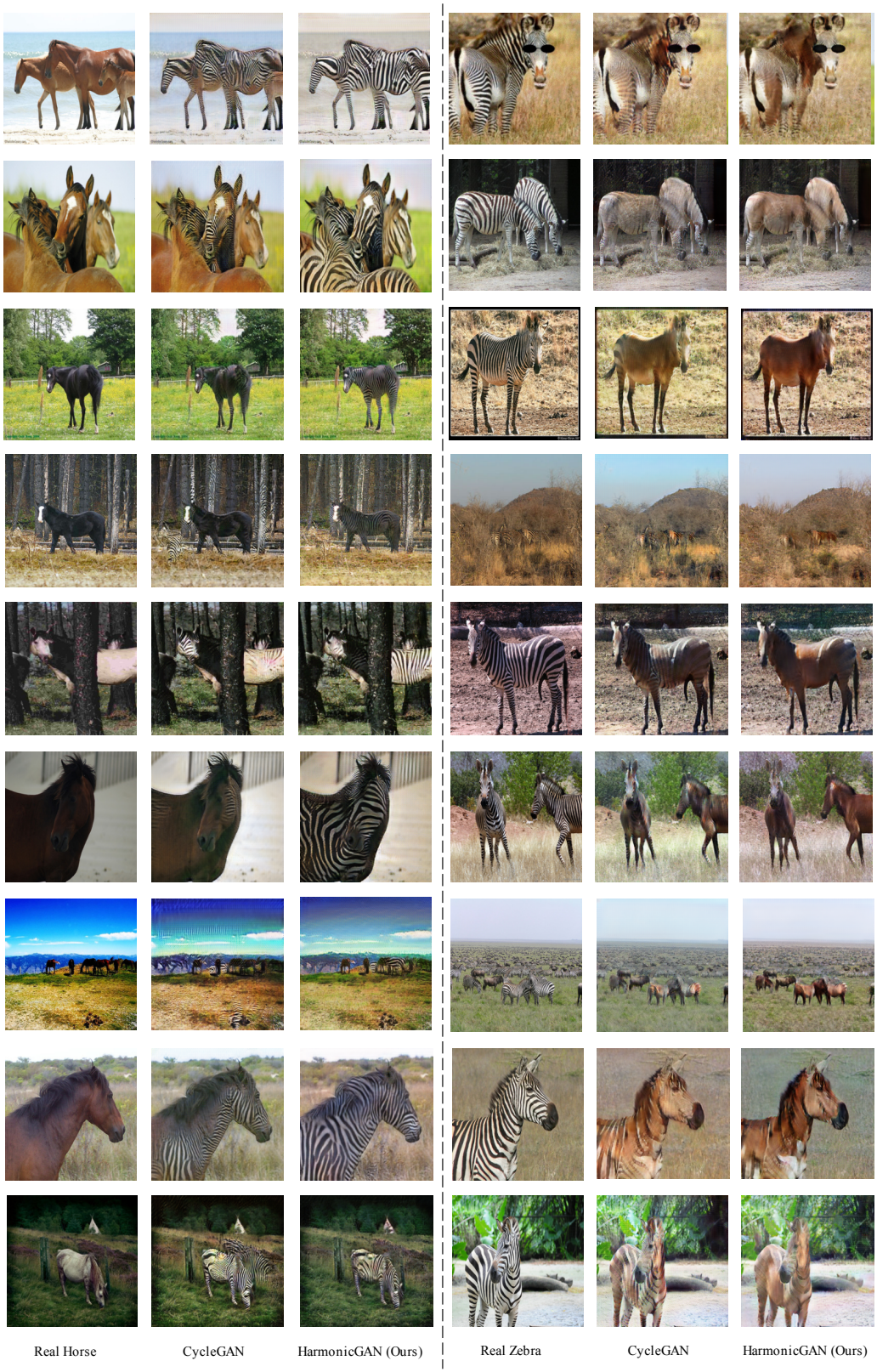

Figure 9: Comparison on horse ↔ zebra.